AGU PUBLICATIONS

JGR

Journal of Geophysical Research: Oceans

RESEARCH ARTICLE

10.1002/2016JC012344

Physical response of a back-barrier estuary to a post-tropical cyclone

A. Beudin[1], N. K. Ganju[1], Z. Defne[1], and A. L. Aretxabaleta[1]

[1]U.S. Geological Survey, Woods Hole, Massachusetts, USA

Key Points:
- Chincoteague Bay response to Hurricane Sandy was simulated with a coupled ocean-wave-sediment model
- Local wind affected bay flow and flushing while remote wind and wave setup controlled water level
- Local waves caused sediment resuspension resulting in bathymetric changes on the order of centimeters

Correspondence to:
A. Beudin,
alexis.beudin@free.fr

Citation:
Beudin, A., N. K. Ganju, Z. Defne, and A. L. Aretxabaleta (2017), Physical response of a back-barrier estuary to a post-tropical cyclone, *J. Geophys. Res. Oceans*, *122*, 5888–5904, doi:10.1002/2016JC012344.

Received 15 SEP 2016
Accepted 13 JUN 2017
Accepted article online 16 JUN 2017
Published online 27 JUL 2017

Abstract This paper presents a modeling investigation of the hydrodynamic and sediment transport response of Chincoteague Bay (VA/MD, USA) to Hurricane Sandy using the Coupled Ocean-Atmosphere-Wave-Sediment-Transport (COAWST) modeling system. Several simulation scenarios with different combinations of remote and local forces were conducted to identify the dominant physical processes. While 80% of the water level increase in the bay was due to coastal sea level at the peak of the storm, a rich spatial and temporal variability in water surface slope was induced by local winds and waves. Local wind increased vertical mixing, horizontal exchanges, and flushing through the inlets. Remote waves (swell) enhanced southward flow through wave setup gradients between the inlets, and increased locally generated wave heights. Locally generated waves had a negligible effect on water level but reduced the residual flow up to 70% due to enhanced apparent roughness and breaking-induced forces. Locally generated waves dominated bed shear stress and sediment resuspension in the bay. Sediment transport patterns mirrored the interior coastline shape and generated deposition on inundated areas. The bay served as a source of fine sediment to the inner shelf, and the ocean-facing barrier island accumulated sand from landward-directed overwash. Despite the intensity of the storm forcing, the bathymetric changes in the bay were on the order of centimeters. This work demonstrates the spectrum of responses to storm forcing, and highlights the importance of local and remote processes on back-barrier estuarine function.

1. Introduction

Back-barrier bays or coastal lagoons are shallow estuaries typically elongated parallel to the coast and connected to the ocean by inlets between barrier islands [*Phleger*, 1969]. During storms, back-barrier estuaries are impacted by offshore water level fluctuations due to wind and pressure forcing, wave setup, local wind-wave sediment erosion and deposition, and barrier island overwash and breaching. While offshore tidal water level fluctuations are typically damped due to inlet constrictions and shallow depths, storm-associated water level fluctuations suffer relatively minor attenuation because inlet friction is less effective to dissipate long-lasting fluctuations [*Garvine*, 1985]. As a consequence, relatively large volumes of the bay are exchanged [*Wong*, 1986] and local wind-waves are modified [*Fagherazzi and Wiberg*, 2009]. Differences in water level between the bay and the ocean drive sediment transport across the submerged portions of the barrier islands [*Sherwood et al.*, 2014], located where the barriers are relatively narrow or urbanized [*Miselis et al.*, 2016]. In addition, (unsteady) wind and wave-current interactions may have local effects that can only be handled by appropriate numerical models [*Signell et al.*, 1990]. The significance of this spatial variability, in comparison to the general mean response of barrier-bay systems to storms, remains to be elucidated.

Chincoteague Bay is located behind Assateague Island astride the states of Virginia and Maryland (Figure 1). The back-barrier bay is approximately 60 km long from Ocean City Inlet in the north to Chincoteague Inlet in the south, with a maximum width of 10 km, and an average depth of 1.4 m (Figure 1b). The watershed area is 315 km^2 (84% of the surface area of the bay). Offshore the tidal amplitude is ~1 m, and the inlets choke the amplitude to ~0.1 m within the bay [*Wang et al.*, 2013]. In the interior of the bay, local wind drives the flow and controls sediment transport through wave resuspension [*Ganju et al.*, 2017]. Surficial bed sediments consist of silt and clay in the deeper western side of the bay adjacent to mainland marshes; the eastern side of the bay is dominated by overwash-derived sand (Figure 1c) [*Wells et al.*, 1997, 1998], creating extensive seagrass habitats dominated by *Zostera marina* (Figure 1d) [*Orth et al.*, 2013].

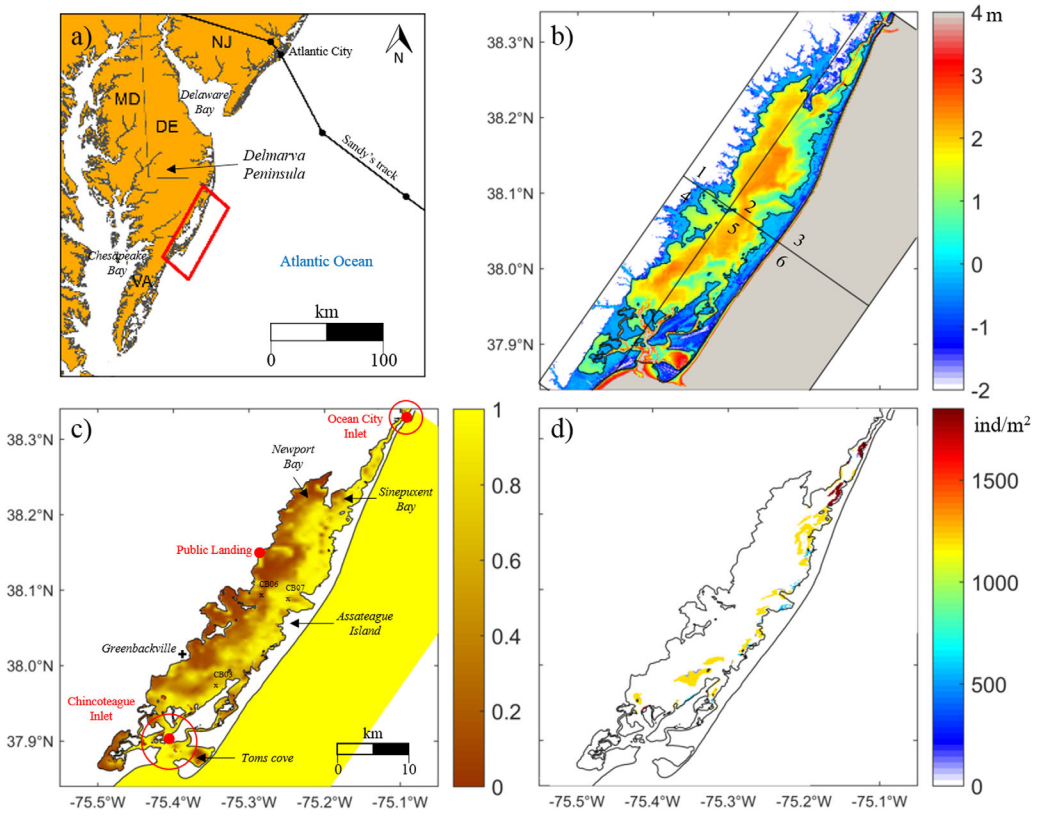

Figure 1. Site maps of (a) model domain location and Hurricane Sandy's track before landing, (b) interpolated topo-bathymetry of Chincoteague Bay and subregions referred to in the text (section 3.2), (c) interpolated sand fraction and geographic locations referred to in the text (the red dots are water level gauges), and (d) interpolated seagrass distribution.

Hurricane Sandy was the second-costliest cyclone to hit the United States on record [*Blake et al.*, 2013] causing at least $50 billion damage. Sandy formed in the central Caribbean on 22 October 2012 and made landfall on 29 October 2012 near Atlantic City, New Jersey [*NOAA*, 2013]. The storm suspended sediment throughout the full water column, formed large scour patches and wave orbital ripples, redistributed sediment on the continental shelf [*Trembanis et al.*, 2013; *Miles et al.*, 2015] and severely eroded the shoreline [*Hapke et al.*, 2013], but little is known about the effects on the numerous back-barrier bays within the Sandy-impacted region, including Great South Bay, New York; Barnegat Bay, New Jersey; and Chincoteague Bay, Maryland/Virginia.

This study investigates the physical response of Chincoteague Bay to Hurricane Sandy using a coupled ocean circulation, wave, and sediment transport numerical model taking advantage of the ability of the model to simulate the spatial heterogeneity of the bay. The model and analysis methods are described in section 2. The simulated bay response in terms of water level, circulation and exchange, bed shear-stress, and sediment transport is quantified and presented in section 3. Last, we discuss the governing processes controlling the physical response (including quantifying the effect of vegetation), with specific attention to the relative importance of remote and local forcing.

2. Methods

2.1. Numerical Modeling System

This study uses the open-source modeling system COAWST (http://woodshole.er.usgs.gov/operations/modeling/COAWST/index.html) that couples the circulation model ROMS, the wave model SWAN, and the sediment transport model CSTMS. While each model is briefly described below, *Warner et al.* [2008, 2010] provide a complete characterization of the modeling suite.

ROMS (Regional Ocean Modeling System) is a three-dimensional, free surface, finite-difference, terrain-following model that solves the Reynolds-Averaged Navier-Stokes equations using the hydrostatic and Boussinesq assumptions [*Haidvogel et al*., 2008]. Wave-induced forces are specified using the vortex force approach [*Kumar et al*., 2012]. Vertical mixing is parameterized with a generic (GLS) two-equation turbulence model [*Warner et al*., 2005]. Bottom shear-stress is calculated using a quadratic drag law and assuming a logarithmic velocity profile in the bottom grid cell [*Warner et al*., 2008], and includes wave apparent roughness [*Madsen*, 1994].

SWAN (Simulating WAves Nearshore) is a third-generation spectral wave model based on the action balance equation [*Booij et al*., 1999]. It simulates wind wave generation and propagation accounting for shifting in relative frequency due to variation in water depth and current (computed by ROMS), depth-induced refraction, wave-wave interactions, and dissipation due to white-capping, depth-induced breaking, and bottom friction. SWAN can also account for diffraction, partial transmission, and reflection.

CSTMS (Community Sediment Transport Modeling System) provides a set of sediment transport routines to compute bed-load and suspended sediment transport rates of various sediment classes, and bed elevation and composition evolution [*Warner et al*., 2008]. Calculations of bed shear-stresses under combined waves and currents follow *Madsen* [1994] and can account for local grain size (provided that the minimum median grain size exceeds 0.6 mm), saltation, and ripple geometry [*Ganju and Sherwood*, 2010].

2.2. Model Setup

2.2.1. Domain and Initial Conditions

The model is run on a 100 m horizontal resolution grid (670 × 300 cells) with seven evenly spaced vertical sigma layers (resulting in an average vertical resolution of 0.2 m in the bay and 2 m offshore), that encompasses the mainland up to an elevation of approximately 10 m (NAVD88), the bay, the barrier island, both inlets, and approximately 15 km of the inner continental shelf (offshore). Topography and bathymetry from a collection of the most recent available data were merged (Figure 1b) [*Wells et al*., 2004; *USACE*, 2013; *USGS*, 2015]. Initially, the water is at rest, with water temperature set to 20°C and salinity set to 30, uniformly across the domain. Water exchange is investigated through the tracking of individual neutral particles ("floats") released every 5 grid points in the bay on 27 October at 12:00 (around the beginning of Sandy). Bed changes and sediment concentration in the water column were tracked for two sediment classes that summarized the sediment fractional distribution from cores and grab samples: one silt class (50 μm) with a settling speed of 1.5 $mm{\cdot}s^{-1}$ and critical shear-stress for erosion of 0.05 $N{\cdot}m^{-2}$; and one sand class (200 μm) with a settling velocity of 21 $mm{\cdot}s^{-1}$ and critical shear-stress for erosion of 0.172 $N{\cdot}m^{-2}$. The bed sediment distribution was initialized using grain-size data collected by *Wells at al*. [1997, 1998] between 1991–1997 in Maryland and 2006–2007 in Virginia (Figure 1c). One bed layer was implemented, with a uniform porosity of 0.5. Seagrass cover (Figure 1d) was specified following the observations of *Orth et al*. [2013].

2.2.2. Forcing and Simulation Scenarios

We simulated the period 15 October to 15 November 2012. The main tidal constituents (K1, O1, M2, N2, and S2) were extracted from the ADCIRC EastCoast2001 tidal database [*Mukai et al*., 2002]. Subtidal water level fluctuations and depth-averaged currents, swell waves, temperature, and salinity were driven at the open-ocean boundary by a large-scale (U.S. East Coast and Gulf of Mexico) COAWST simulation [*Warner et al*., 2010]. Harmonic analysis of water levels and currents were carried out with T_TIDE [*Pawlowicz et al*., 2002]

Table 1. Model Scenarios (the NonS Scenario Is Not Listed; Its Forcing Is Made From the Forcing for the Scenario S With the Event Filtered-Out of the Low-Pass Signals)

Name	Tides	Offshore Subtidal Water Level Fluctuations	Atmospheric Forcing (Pressure and Wind)	Locally Generated Wind Waves	Offshore Swell	Seagrass
S	x	x	x	x	x	
T	x					
TS	x	x				
TA	x		x			
TSA	x	x	x			
TSAW	x	x	x	x		
TSAS	x	x	x		x	
SAV	x	x	x	x	x	x

Table 2. Model Skill Assessment for Water Level, Wave Height, and Combined Wave-Current Bottom Shear-Stress at Three Instrumented Stations (Located in Figure 1c) Over the November 2014 to February 2015 Period [*Suttles et al*., 2016; *Ganju et al*., 2017][a]

	Water Level			Wave Height			Bottom Shear-Stress		
Station\Skill	R^2	RMSE (m)	BSS	R^2	RMSE (m)	BSS	R^2	RMSE (Pa)	BSS
CB03	0.65	0.14	0.42	0.58	0.08	0.15	0.38	0.16	0.03
CB06	0.46	0.16	0.02	0.53	0.09	0.38	0.42	0.13	0.42
CB07	0.49	0.16	0.09	0.51	0.07	−0.47	0.35	0.24	0.35

[a]Brier Skill Score (BSS) vary between 1 and $-\infty$, a value greater than 0 indicates a time-varying prediction that is better than time-averaged mean value.

to generate the subtidal (detided) forcing at the open-ocean boundary. Freshwater and sediment inputs from land were considered negligible at this period of the year [*Pritchard*, 1960]. Atmospheric forcing (wind velocity, air pressure, and solar radiation) was obtained from the weather model NCEP NAM 12 km horizontal resolution [*NOAA*, 2012].

The reference simulation (scenario S for Sandy) is compared to a control simulation in which the storm event has been filtered out from the forcing (scenario nonS or non-Sandy). To identify the storm event, the subtidal water level and current velocity along the open-ocean boundary were calculated by applying a low-pass filter with a 1/30 h^{-1} cutoff frequency. The portion of the low-frequency signals around the peak of the storm between two local minima is replaced by a linear interpolation between the two minima. The same procedure was applied to atmospheric forcing (wind velocity and air pressure) with a cutoff frequency of 1/12 h^{-1} (to retain the sea breeze), and to offshore waves (height and period) with a cutoff frequency of 1/48 h^{-1}. A set of simulations (Table 1) was used to quantify the effects of each forcing (remote subtidal water level fluctuations, wind, and waves), and the influence of seagrass. The SAV simulation included the wave-flow-vegetation interaction model [*Beudin et al*., 2017] using an upright seagrass blade height of 30 cm, blade width of 0.3 cm, blade thickness of 0.3 mm, tissue density of 700 $kg{\cdot}m^{-3}$, and elastic modulus of 1 GPa [*Luhar and Nepf*, 2011] (J. Testa, personal communication, 2015). The ROMS barotropic and baroclinic time steps were, respectively, 0.1 s and 2 s, while the SWAN time step and the coupling interval between ROMS and SWAN were 10 min.

2.2.3. Analysis Techniques

As observations during the occurrence of Sandy were limited to water level measurements, model verification during Sandy was based on the available data at three locations in the bay using standard performance metrics: Brier's skill score (BSS), Pearson's correlation coefficient squared (R^2), and root-mean-square error (RMSE). Additionally, *Ganju et al*. [2017] simulated the November 2014 to February 2015 period and provided comparisons at three stations in the bay (for bed level change). The 2014–2015 instrumented stations, described by *Suttles et al*. [2016], have been used to establish the skill of the model for water level, wave height, and combined wave-current bottom shear-stress (Table 2). Particle tracking within the ROMS model, using neutrally buoyant particles, was used to quantify spatially variable residence time, defined as time elapsed before particles exit the bay [*Defne and Ganju*, 2014], and time-dependent connectivity among subregions [*Defne et al*., 2016]. Particle exchanges between subregions were summarized in a source-destination matrix of retention clocks showing the change in particle concentration through time. Here, the model domain was split in six subregions: quadrants of the bay and north-south divisions of the offshore region (Figure 1b). This delineation allows clear separation between the north and the south of the bay as well as the influence of the inlets and exchanges between the relatively deep western side and the shallower eastern side.

3. Results

3.1. Water Level

Modeled water levels captured much of the observed subtidal and tidal fluctuations, with a BSS exceeding 0.7 at all sites (Figure 2). Tidal fluctuations in the interior of the bay were highly dampened, while subtidal fluctuations displayed little reduction in amplitude but a phase lag up to 12 h relative to the inlets. As opposed to a simple bathtub-like filling and draining, water levels in the bay showed distinct spatial and temporal variability. Storm surge (defined as the Sandy-induced water level, i.e., difference of water level

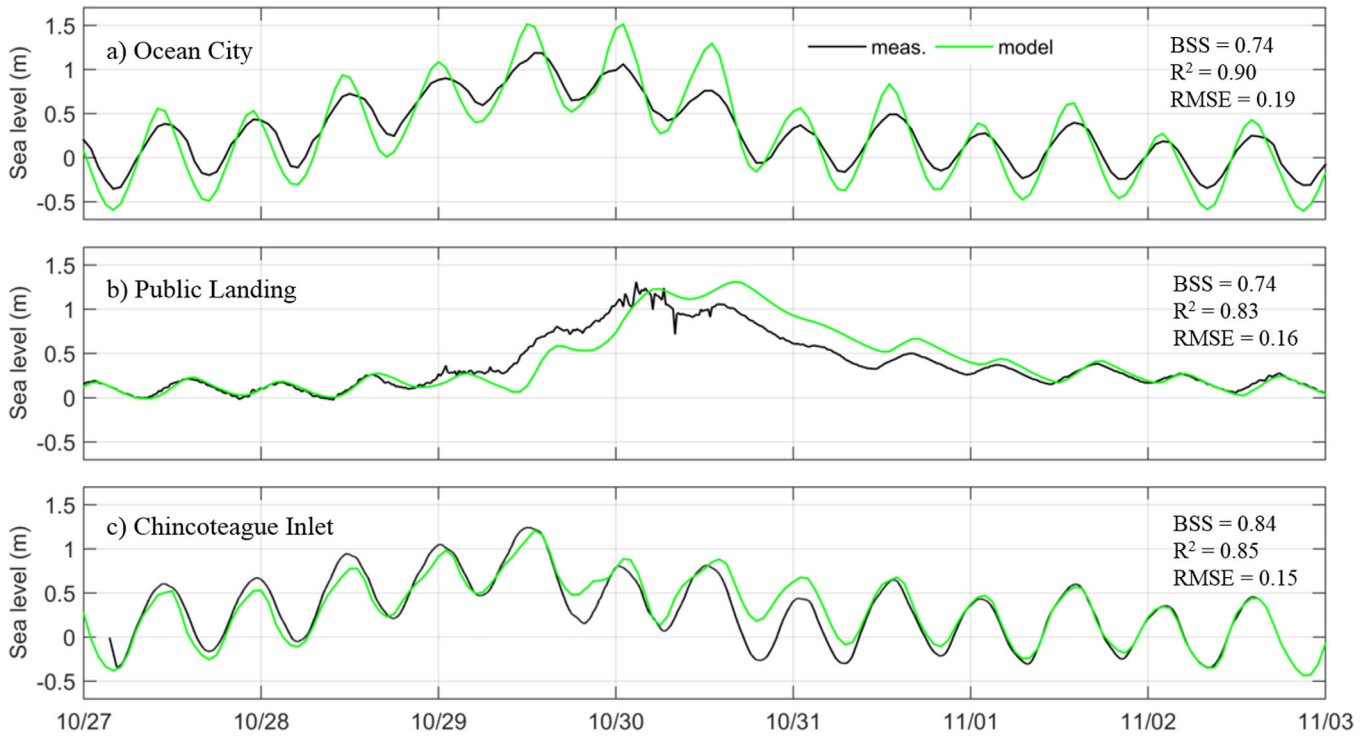

Figure 2. Time series of measured and simulated water level fluctuations at (a) Ocean City NOAA station (longitude: −75.0917, latitude: 38.3283), (b) Public Landing Maryland DNR station (–75.2862, 38.1483), and (c) Chincoteague Bay USGS storm tide sensor (–75.4067, 37.9032), between 27 October and 3 November 2012.

between the S and nonS model scenarios) exceeded 1 m inside the inlets (Figure 3a). Surge levels exceeded 0.8 m in more than 75% of the bay, and the smallest surge was located in the southwest of the bay where peak values were ∼0.7 m. The average peak surge was ∼0.9 m in the bay and slightly less (0.8 m) offshore. The model simulated inundated mainland and barrier island area increased the wetted area of the bay by ∼50%. The period of "highest surge" (when the surge exceeded the 0.7 m lower envelope in the bay) lasted less than 30 h in most of the bay, except in the northern inlet and on the eastern side of the bay where it lasted ∼36 h (Figure 3b). Considering a lower surge threshold (0.5 m), the southern part of the bay experienced much longer surge exposure than the northern part (48 versus 24 h). The contribution of each storm forcing to water level in the bay is presented in section 4.

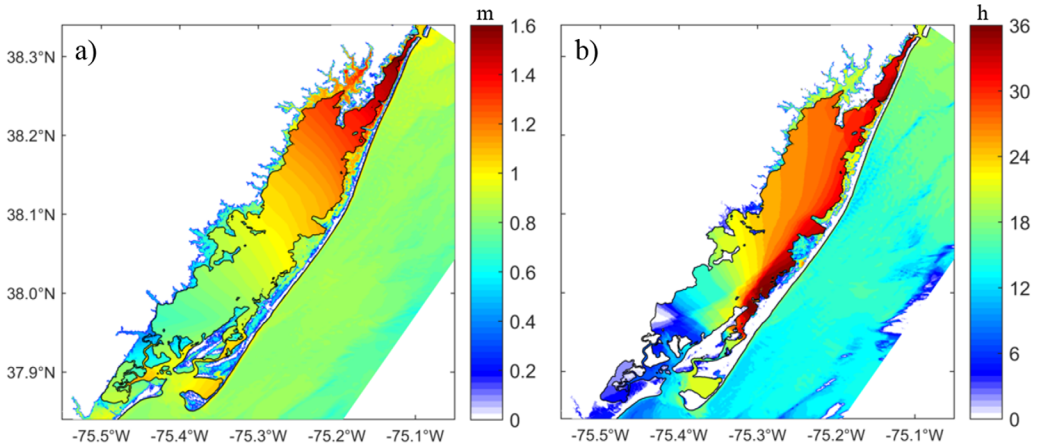

Figure 3. Maps of (a) maximum Sandy-induced water level anomaly (surge) and (b) duration of "highest surge" defined as the time when the Sandy-induced water level anomaly exceeds 0.7 m.

3.2. Water Exchange

The percentage of model floats exported from the bay (within 18.5 days after the release) increased from 15% (with scenario nonS) to 40% (with scenario S). Ninety percent of those floats were exported between 29 October and 2 November, and by that time, the number of exported floats was 4 times larger than in the nonS case. Sixty five percent of the total exported floats escaped through Chincoteague Inlet, with 99% of those floats originating from the southern region of the bay (R4–R5 in Figure 1b). Meanwhile, 95% of the floats exported through Ocean City Inlet originated from the northern region of the bay (R1–R2 in Figure 1b). The northwestern region (R1) was the least flushed: 15% of the floats initially in this quadrant were exported, while 40, 30, and 35% of the floats from the northeast (R2), southwest (R4), and southeast (R5), respectively, were exported out. Residence time was reduced overall in the bay with Sandy (by 4 days), but increased locally in the northern inlet and the southern basin compared to the non-Sandy simulation (Figure 4a). Cross-bay averaged residence time was reduced by 10 days at a distance of 10–20 km from the mouth of both inlets (Figure 4b). This value is considerable given that the average flushing time of the bay (simulated with the nonS scenario) ranged between 40 (extrapolated with an exponential decay best fitted to data) and 95 days (double exponential decay best fit; [*Defne and Ganju*, 2014]), and it is in reasonable agreement with the 2 month estimate of *Pritchard* [1960]. Sandy conditions enhanced water exchange between the bay and the inner continental shelf, as well as the exchanges within the bay.

The retention clock matrix shows the time variability of the exchanges among quadrants of the bay and to the two subregions offshore of the inlets (Figure 5). The northwest subregion (R1) was the least retentive during Sandy, followed by the southeast subregion (R5), with the northeast subregion (R2) being the most retentive by the end of the storm. Exchanges between northern and southern subregions were on the order of 15–20% of the total floats originally released (e.g., 20% of floats from R1 were transported to R4 during the first 2 days of Sandy, 15% of floats from R4 drifted to R2 during the last 42 h of the storm, 20% of floats from R5 reached R2 after the first 2 days). Lateral exchanges between eastern and western subregions were much larger and usually exceeded half of the released particles (e.g., 60% exchange from R1 to R2 during the storm, 50% of floats from R5 to R4 during the first 2 days). The export of particles from the different

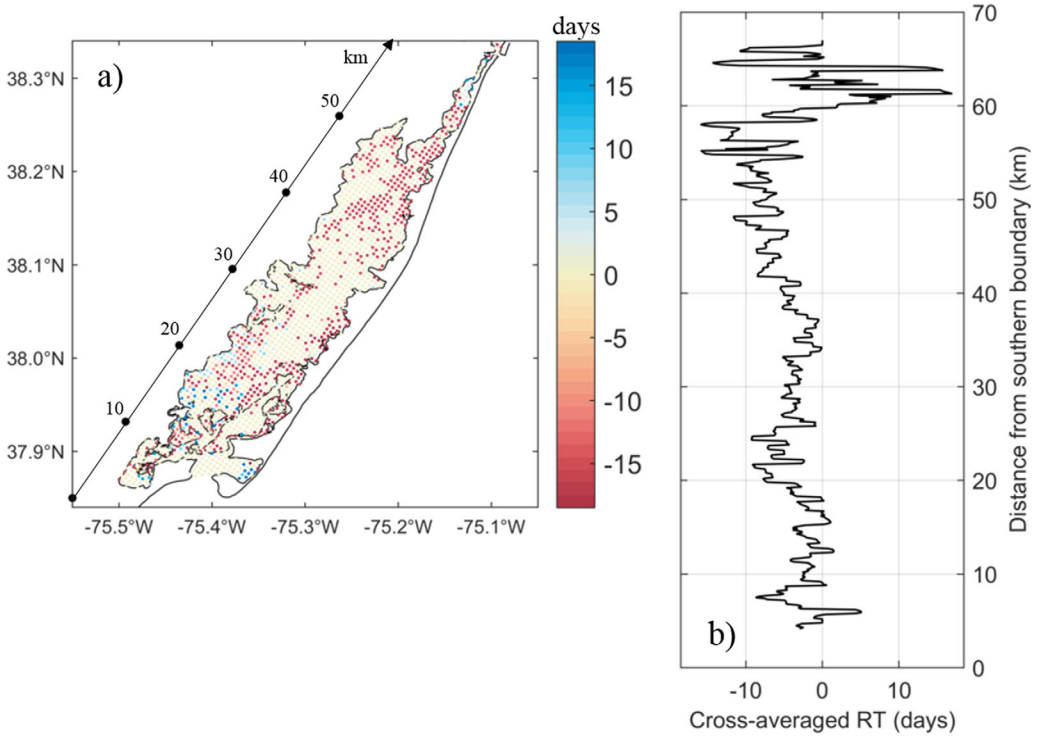

Figure 4. Residence time difference between the S and nonS scenarios: (a) at each float initial location, and (b) along the bay (cross-averaged). The values are limited by the length of the simulation after the release of the floats (18.5 days).

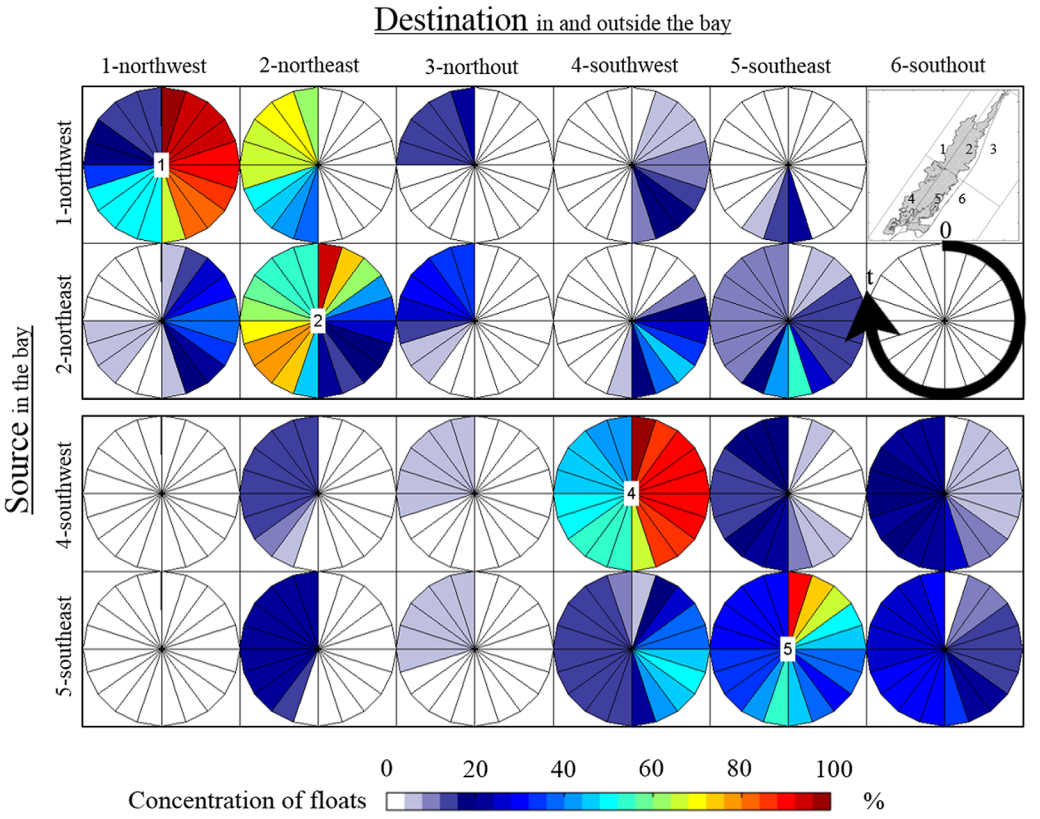

Figure 5. Retention clock matrix for six subregions (R1–6) of the model domain (see inset plot at the top-right corner and in Figure 1b). The floats are transported from source (row) to destination (column). The time t progresses clockwise with a 6 h interval (half a semidiurnal tidal cycle) during the 5 days of Sandy (27 October to 1 November). Float concentration in each subregion (number of floats at time t divided by initial number of floats in the source subregion) reflects their retention characteristics.

subregions to the offshore through the inlets ranged from 5% from R5 through Ocean City Inlet (R3) to 30% from R4 through Chincoteague Inlet (R6). The timing of the exchanges between subregions was controlled by the shifting wind direction with initial (first 2 days) east-to-west migration, followed by north-to-south transport (34–60 h), then a shift west-to-east (48–72 h) and finally a predominantly northward migration. The matrix distribution was consistent with a counterclockwise rotating flow in the bay during Sandy. A large contribution to the variability in lateral exchange between subregions was due to semidiurnal tidal fluctuations.

3.3. Bed Shear-Stress and Sediment Transport

The model total (combined wave-current) bed shear-stress averaged over the bay increased by an order of magnitude from ~0.1 to 1.3 $N{\cdot}m^{-2}$ under Sandy conditions (Figure 6d). The wave contribution was enhanced from ~0.05 to 1 $N{\cdot}m^{-2}$, while the current-induced shear-stress increased from ~0.1 to 0.4 $N{\cdot}m^{-2}$. At the peak of Sandy, the wave contribution dominated over the current contribution everywhere except in the deeper channels and over some inundated areas (Figure 7a). The non-Sandy conditions were dominated by wave-stress in the north and current-stress in the south (stronger tidal flow in Chincoteague Inlet). The cumulative (total) bed shear-stress throughout the course of Sandy showed a band of enhanced stress (up to 4.5 $N{\cdot}m^{-2}{\cdot}d$) on the eastern shoals (Figure 7b). While the values in the bay are significantly increased during the storm, the values overall are smaller than offshore. In both inlets, dominated by current-stress, the cumulative bed shear-stress was either only slightly increased or decreased (by less than 20%) compared to the non-Sandy case. Using the relationship between cumulative excess shear-stress (above the critical shear-stresses for sediment erosion) and bed elevation change observed in Chincoteague Bay during the year 2014/2015 [*Ganju et al.*, 2017], the cumulative excess shear-stress above the critical shear-stresses for erosion of silt (0.05 $N{\cdot}m^{-2}$) and sand (0.172 $N{\cdot}m^{-2}$) indicated that the erosion caused by Sandy would be less than 6 cm (maximum value on the eastern shoals).

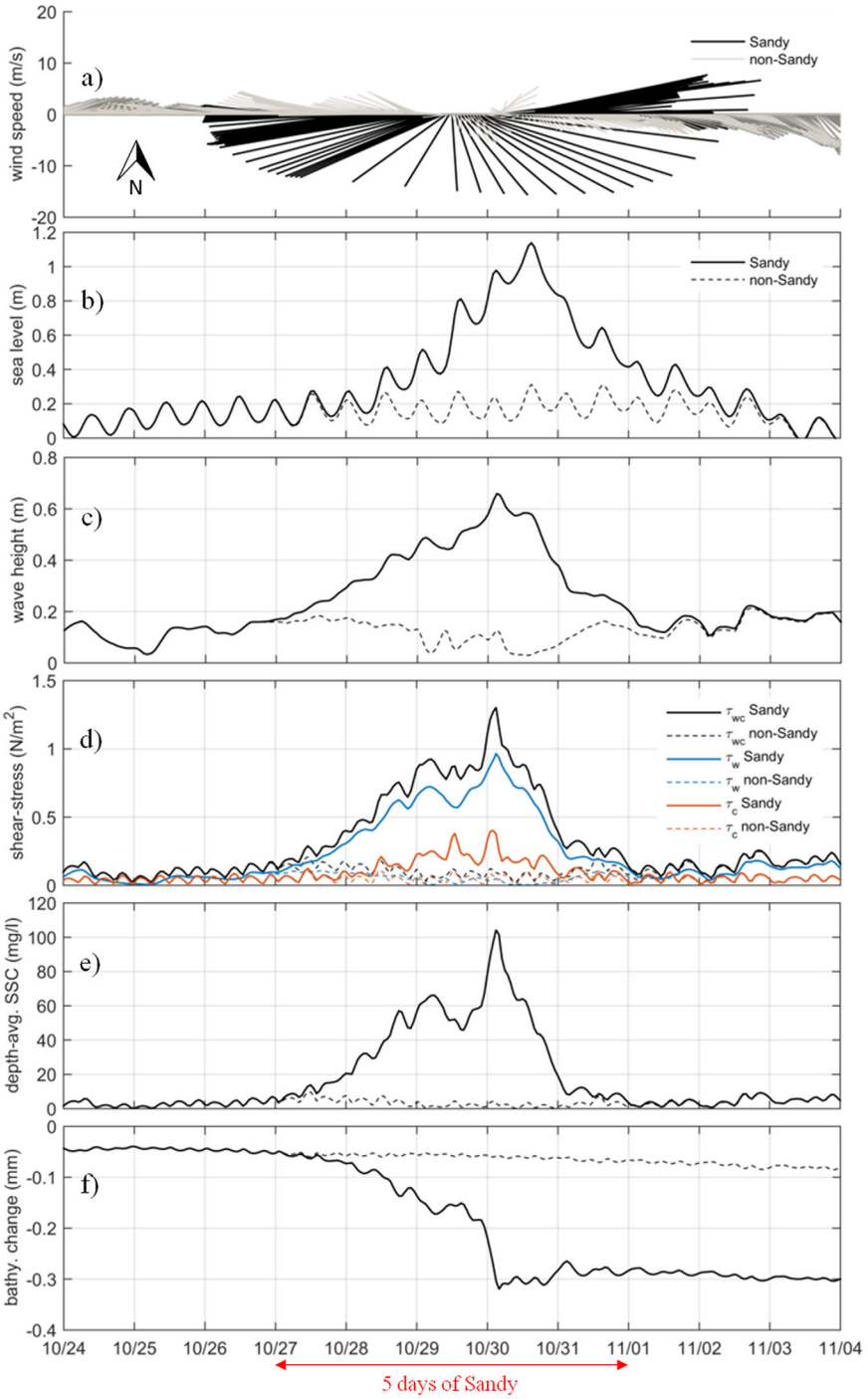

Figure 6. Bay-averaged (a) wind speed and direction, (b) water level fluctuation around MSL, (c) significant wave height, (d) bed shear-stresses (τ_{wc}: combined wave-current, τ_w: wave-alone, τ_c: current-alone), (e) depth-averaged suspended sediment (silt plus sand) concentration, and (f) bathymetric change, with the Sandy and non-Sandy scenarios between 24 October and 4 November.

The bay and depth-averaged SSC exceeded 100 mg·L^{-1} as compared to 10 mg·L^{-1} in the non-Sandy case (Figure 6e), and displayed a double peak in phase with wave-induced bed shear-stress occurring with NE and SW wind directions (longest fetches). The ratio between near-bottom and near-surface SSC decreased (from around 4 to 2 with apparently less tidal fluctuations) during Sandy, but increased (by 20%) on the aftermath of the storm (31 October to 1 November) as sediment settled through the water column. SSC peaked in the south of the bay as a result of locally stronger bed shear-stress (Figure 7a) and a relatively

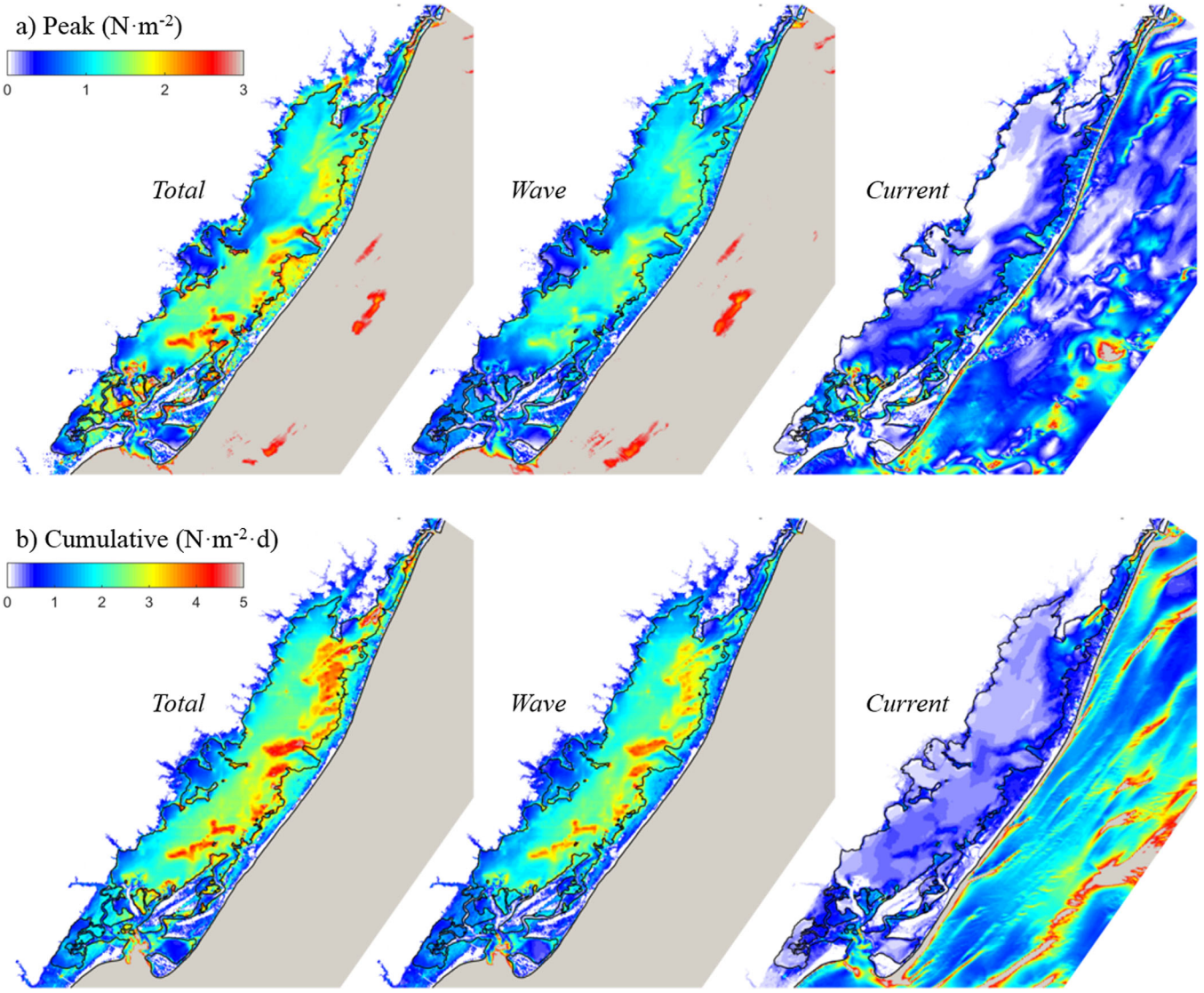

Figure 7. Total (combined wave-current), wave-alone, and current-alone bed shear-stresses induced by Sandy (difference between the S and nonS scenarios), (a) at the instant of maximum wind stress (Figure 6), and (b) cumulated during the 5 days of Sandy (27 October to 1 November).

higher silt fraction (Figure 1c). SSC in the water column was dominated by the silt fraction, except over the eastern shoals where the bed is composed primarily of sand. Model suspended sediment flux was amplified (by a factor 6) as compared to the non-Sandy case, principally in the deeper channels and northern region of the bay, corresponding with larger water flux (Figure 8). The direction of suspended sediment flux differed from the mean flow direction: northward in the southern basin and westward in the middle bay, while the mean flow overall was to the south. This indicates that the dense cloud of suspended sediment in the south was transported predominantly by diffusion rather than advection. Bedload flux, dominated by the sand fraction, was smaller than suspended flux on average in the bay, but larger in the northern inlet and on the eastern shoals, and generally directed southward (Figure 8c). The total sediment fluxes from the control volume of the bay (Table 3) indicated that Chincoteague Bay lost sediment, primarily silt, while Assateague Island gained sediment, essentially sand from the seashore. The maximum overall erosion in the bay was estimated during the peak of bed shear-stress, and contrary to the other physical components, the overall bed thickness did not return to prestorm values (Figure 6f). As expected from the values of cumulative excess shear-stress and sediment flux, the bathymetric changes in the bay were of the order of centimeters (Figure 9). Locally, erosion often occurred in the proximity of the tips of the headlands and deposition in the shadows, from which arose striped sedimentation patterns following the indentation of

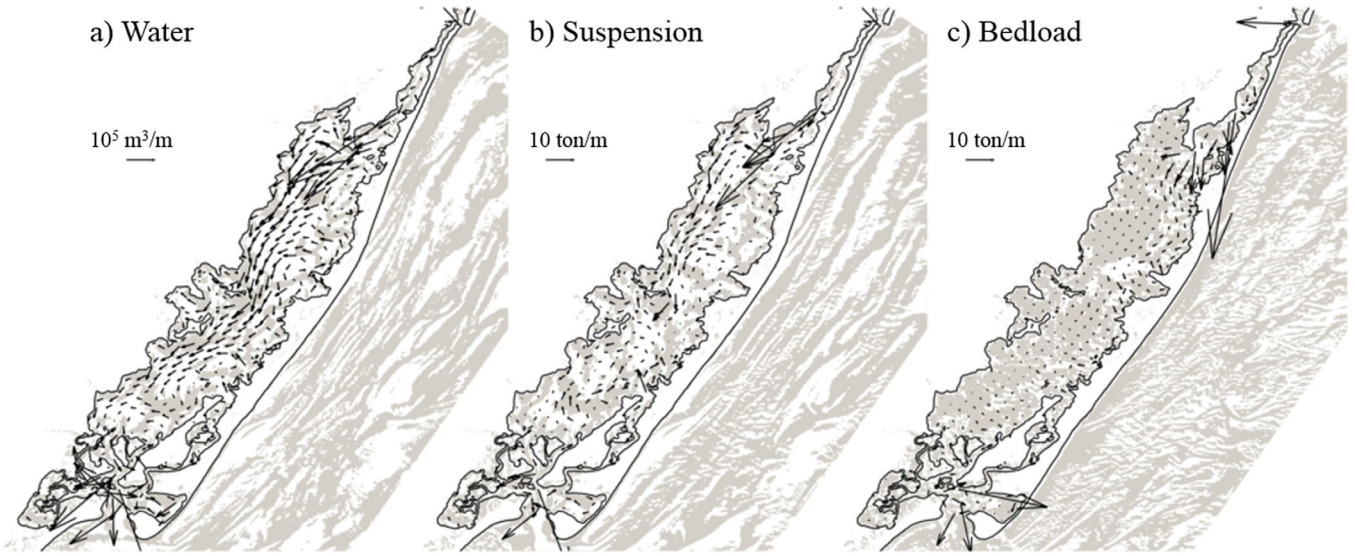

Figure 8. Fluxes (per unit width) of (a) water, (b) suspended sediment, and (c) bedload sediment, cumulated during the 5 days of Sandy (27 October to 1 November), plotted (1 arrow every 10 grid points in the bay) on top of the sign of the vector field divergence to show the fine-scale circulation patterns (the fluxes point inward in the gray area).

the coast at kilometer-scale (Figures 9a and 9a'). Overall, most erosion occurred within 0 and 1 m depth due to larger wave-induced shear-stress (while erosion in the deeper region was related to current-induced shear-stress), and most deposition occurred between 0 and 1 m above mean sea level (Figure 9c). The northeastern region underwent the largest bathymetric change (Figures 9a and 9b) and on average was more depositional as a result of barrier overwash. Similar depositional features behind the barrier were observed in Barnegat Bay, New Jersey, after Hurricane Sandy [*Miselis et al*., 2016].

4. Discussion

4.1. Dominant Forces and Processes

The effect of stratification in Chincoteague Bay during Sandy was almost negligible as the bay is relatively shallow and the total cumulative rainfall (on the watershed and on the bay) did not exceed 5% of the bay water volume. The gradient Richardson number ($Ri = g\frac{\partial\rho}{\partial z}/\rho\left(\frac{\partial u}{\partial z}\right)^2$ with g being gravity, ρ being density, and u being current speed) in the bay ranged from 0 to 0.2 with most values being close to zero. Under these circumstances, mixing completely dominated over stratification. While under more stratified estuarine conditions, a decoupling between near-surface and near-bottom processes is expected [*Noble et al*., 1996], the conditions in Chincoteague Bay during Sandy prevented the occurrence of such decoupling and resulted in well-mixed vertical profiles.

The depth-averaged momentum balance (Figure 10) was dominated by pressure gradient force (bay-average $\mu = 1.18{\cdot}10^{-4}$ m·s^{-2}), wind stress ($\mu = 6.37{\cdot}10^{-5}$ m·s^{-2}), bottom friction ($\mu = 4.16{\cdot}10^{-5}$ m·s^{-2}), and wave-induced breaking force ($\mu = 2.65{\cdot}10^{-5}$ m·s^{-2}). In the cross-bay direction (x axis), the pressure gradient force was balanced by bottom friction in the inlets with local variations mirroring the complex channel-shoal geometry. Wind stress was balanced by the pressure gradient force in the interior of the bay, while pressure gradient and wave-induced breaking forces dominated on the eastern shoals. The pressure gradient and breaking force directions in the bay and offshore were opposite. In the along-bay direction (y axis), wind stress was balanced by bottom friction on the north-eastern shoals, and by pressure gradient

Table 3. Total Sediment Flux Cumulated During the 5 Days of Sandy (27 October to 1 November)[a]

Section	Sediment Flux (ton)	Percent of Sand
Mouth of Chincoteague Inlet	$-1.7{\cdot}10^4$	70
Mouth of Ocean City Inlet	$-1.3{\cdot}10^4$	10
Mainland/Bay*	$-6.4{\cdot}10^3$	20
Bay/Barrier*	$-6.3{\cdot}10^3$	50
Barrier/Offshore*	$+1.1{\cdot}10^6$	99

[a]Negative means export from the bay, and vice versa. (*: mean sea level).

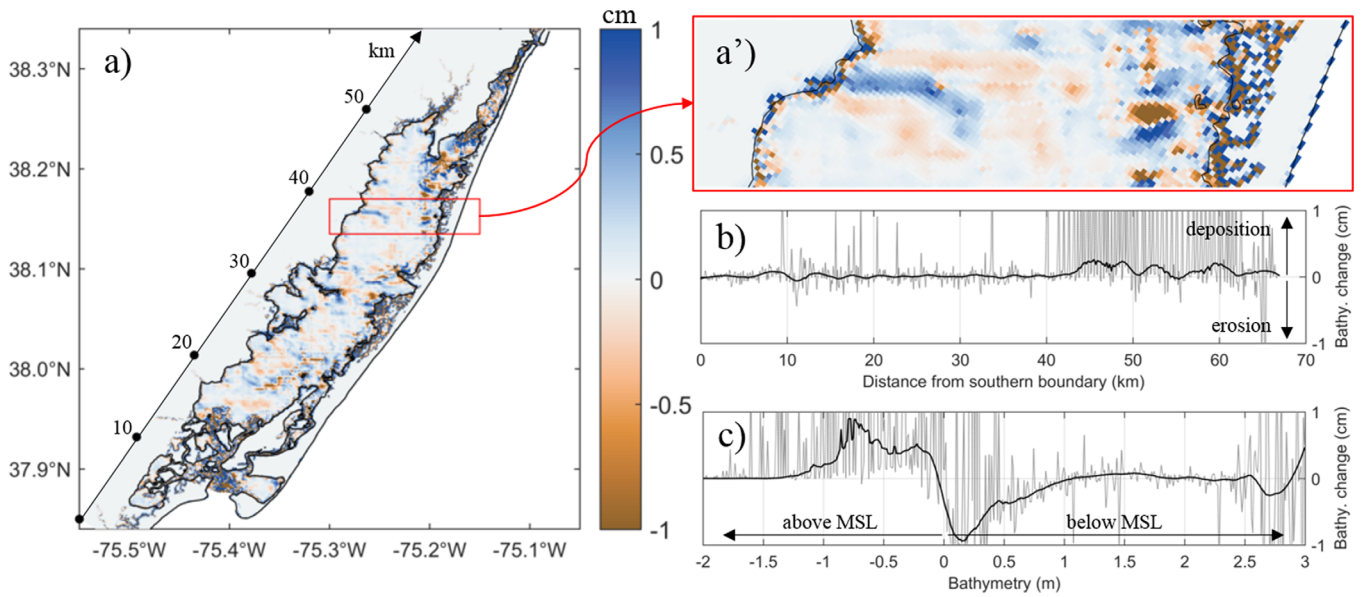

Figure 9. Bathymetric change induced by Sandy (difference between the S and nonS scenarios): (a) throughout the bay (a': zoom), (b) along the bay (cross-averaged), and (c) clustered as a function of bathymetry. Positive (blue) and negative (brown) bathymetric changes mean deposition and erosion, respectively.

force on the north-western basin, while pressure gradient force and bottom friction dominated in the inlets.

Pressure gradient was induced by local wind setup and remote wave setup. At the peak wind stress (30 October 3:00), water level change between scenarios TA (tidal and atmospheric forcing only) and T (tidal forcing only) reached 0.4 m in the northern inlet and −0.9 m in the southern basin (water surface

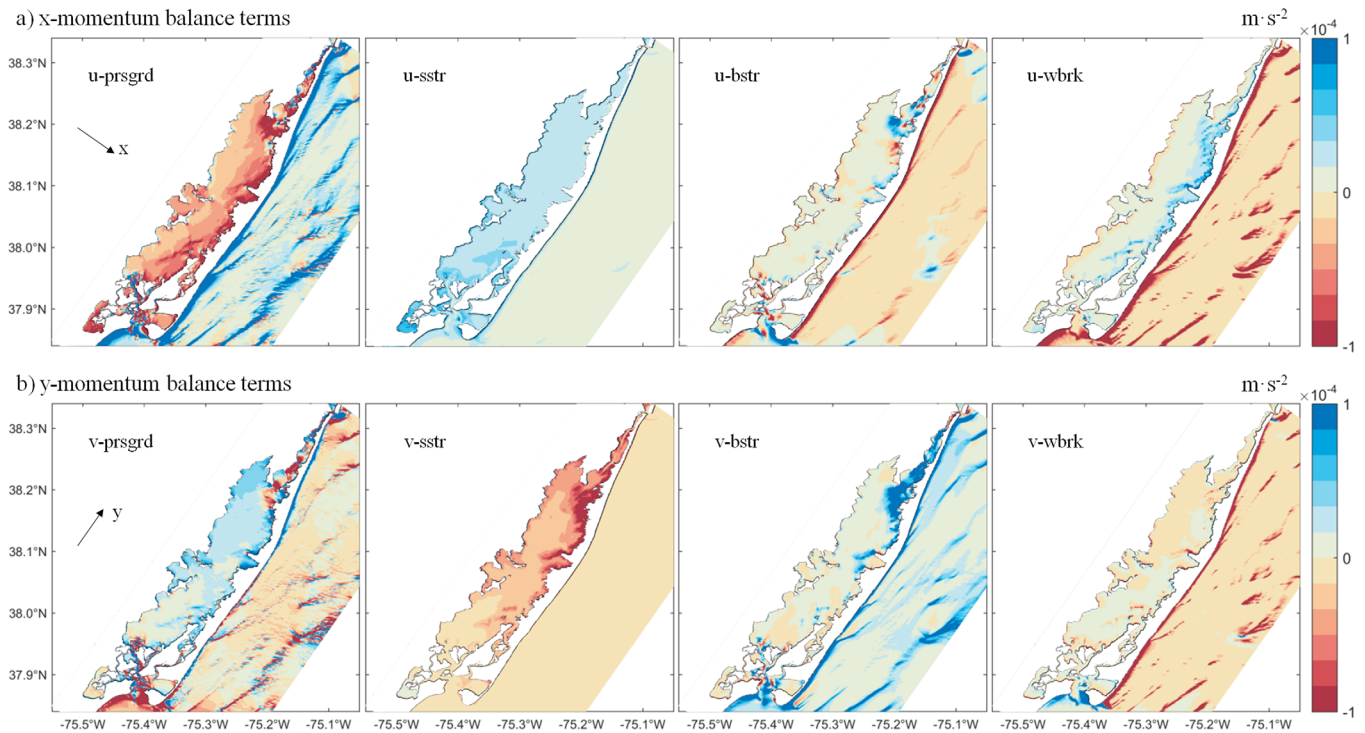

Figure 10. Leading terms in the depth-averaged momentum balance equations (along *x* and *y*, respectively) averaged during the 5 days of Sandy (27 October to 1 November). (prsgrd: pressure gradient, sstr: surface stress, bstr: bottom stress, and wbrk: wave breaking.)

slope $\sim 3 \cdot 10^{-5}$). The depth-integrated momentum equation along the principal axis of the bay axis: $\frac{\partial \eta}{\partial y} = \frac{\tau}{\rho g h}$ provides the same slope with $\tau = 0.9\ \mathrm{N \cdot m^{-2}}$ (peak wind stress) and $h = 3\ m$ (water depth in the channel). At the peak wave height offshore (29 October 16:00), water level change between scenarios S and TSAW (no swell offshore) reached 0.55 and 0.25 m in the north and south inlets, respectively. Wave setup is a response to wave height decrease at the coast [*Longuet-Higgins and Stewart*, 1964], and the difference of setup between the two inlets reflected the offshore spatial gradients in wave height and bathymetric slope. In the case of large waves in shallow water, wave setup can be reduced to $\eta = \frac{a^2}{4h}$ [*Longuet-Higgins and Stewart*, 1964] where a is the wave amplitude and h the water depth. Assuming that waves break at the mouth of the inlets, their height is proportional to water depth such as $a = 0.73\ h$ [*Eldeberky and Battjes*, 1996; *SWAN Team*, 2015], and therefore, wave setup is limited to ~10% of water depth at the mouth of the inlets. According to this simple formulation and given that the average depth in Ocean City Inlet and Chincoteague Inlet is 6 and 3 m, wave setup was around 0.6 and 0.3 m, respectively (by comparison the numerical model predicted 0.55 and 0.25 m, respectively). Similar contribution from wave setup to surge levels was reported in Great South Bay, New-York [*Irish and Cañizares*, 2009].

Remote subtidal sea level fluctuations did not directly affect the momentum balance, but they were responsible for 80% of the simulated maximum water level in the bay (peak on 30 October 4:00) and as such had other important influences. The combination of subtidal sea level fluctuations and wave setup induced overwash in the narrowest sections of the barrier island (northern section and locally at the south in Toms Cove). The difference in water discharge between the different simulation scenarios (Figure 11) revealed that the main forcing was remote swell waves, and that locally generated waves significantly reduced the flow (up to 70% in Chincoteague Inlet). This result differs with the hydrodynamic response to more common storms dominated by sustained winds along the bay, in which case the flow is downwind on the shoals and upwind on the deeper channel [*Ganju et al*., 2017]. *Olabarrieta et al*. [2011] also showed that during storm conditions wave setup had a larger effect on water level and currents than local wind in a large macrotidal coastal plain estuary (Willapa Bay, WA). The gradient of wave setup between the two inlets of Chincoteague Bay during Sandy increased the (southward) flushing of the bay, while wave setup at the mouth of the single inlet of Willapa Bay reduced the flushing of estuarine water.

Remote forcing dominates subtidal water level fluctuations and (often) flushing of back-barrier bays [*Wong*, 1986; *Wong*, 1987; *Smith*, 2001; *Chant*, 2001; *Defne and Ganju*, 2014], while local processes control transport and distribution of waterborne material [*Wong and Moses-Hall*, 1998], in particular sediments. The contribution of locally generated waves accounted for 70–80% of the total bed shear-stress on average in

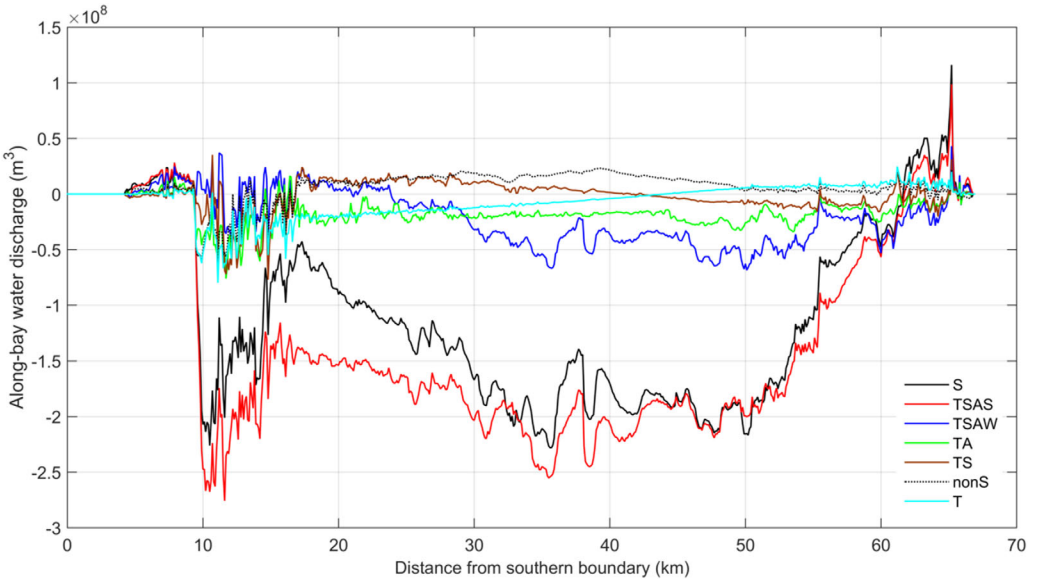

Figure 11. Water discharge (water flux integrated across the bay) during the 5 days of Sandy (27 October to 1 November) with the different simulation scenarios (Table 1): S (complete Sandy scenario), TSAS (no wind waves), TSAW (no swell), TA (tidal and atmospheric forcing), TS (tidal and subtidal sea level fluctuations), nonS (non-Sandy), and T (tide only).

Chincoteague Bay during Sandy (Figures 6d and 7) and during winter storms [*Ganju et al.*, 2017]. Wave erosion occurred mainly in areas located between 0 and 1 m below mean sea level, and this sediment deposited above mean sea level on the inundated areas (up to ~1 m elevation; Figure 9).

The comparison between the S and TSAW (no swell) scenarios revealed that locally generated waves were significantly enhanced by remote wave forcing. At the peak of wind stress (30 October 3:00), the wind was blowing from the southwest generating waves of ~1 m (3–4 s) in the northern basin with scenario S, but only 0.2 m (1–2 s) in the middle of the bay with scenario TSAW. Remote wave forcing increased water level in the northern portion of the bay by 0.4–0.5 m, increasing depth-limited wave height by 0.3–0.35 m (a=0.73 h=0.73×0.4=0.3 m). Wave setup in Chincoteague Inlet also led to longer fetch as the marsh platform (in the southwest) was fully submerged. In addition, remote wave forcing generated a gradient of wave setup between the two inlets creating a pressure gradient force in the opposite direction to wind stress, reducing the downwind current velocity (by 30% on the northeastern shoals up to 60% in the middle of the bay). Wave height was increased due to slower currents following the wave action balance equation: $\frac{\partial A}{\partial t}+\frac{\partial}{\partial x}\left(\left(U+c_g\right)A\right)=0$ with $A=\frac{0.5\rho g a^2}{\sigma}$ the wave action, a the wave height, σ the intrinsic (relative) wave frequency, and U the current velocity (positive in the direction of wave propagation). In summary, the overall physical response of Chincoteague Bay to Hurricane Sandy was dominated by remote and local waves, the former significantly influencing the latter.

4.2 Influence of Seagrass

As model skill for water level (Figure 2) was not improved with the inclusion of seagrass, vegetation effects were not included in the previous sections. Overall, water level was not significantly affected by seagrass (less than 1% difference on average), yet seagrass reduced water level by 10% in the northern channel and increased it by 2% in the south during peak water level conditions (30 October 16:00). Model depth-averaged velocities were reduced by 10% on average over the seagrass meadows, which is roughly equivalent (assuming the pressure gradient was unchanged) to increase the bed friction coefficient (including wave apparent roughness) by 25% to account for the drag of seagrass. In fact, the present three-dimensional parameterization of vegetation provides a more physically appropriate approach to simulate shear flows and turbulent mixing than a simple drag increase parameterization. Seagrass effects included: the water transport along the bay being reduced by 10%; the number of floats exported from the bay being reduced by 20%; and the bay-averaged residence time being increased by 10% with seagrass.

Wave damping occurred locally on the seagrass meadows (more than 5% wave height reduction within approximately 1 km, Figure 12a). Waves in the bay during Sandy were depth-limited and not wind-limited, so they were able to grow (regenerate) rapidly. Nevertheless, seagrass has the potential to reduce wave attack on marshes, as waves propagating from the bay through the meadows and into the marsh would be attenuated. Wave height was reduced by 30–75% on the meadows, and 5% on average in the bay (40% in the north, and increased by 2% in the south). The model estimates of wave damping by vegetation should

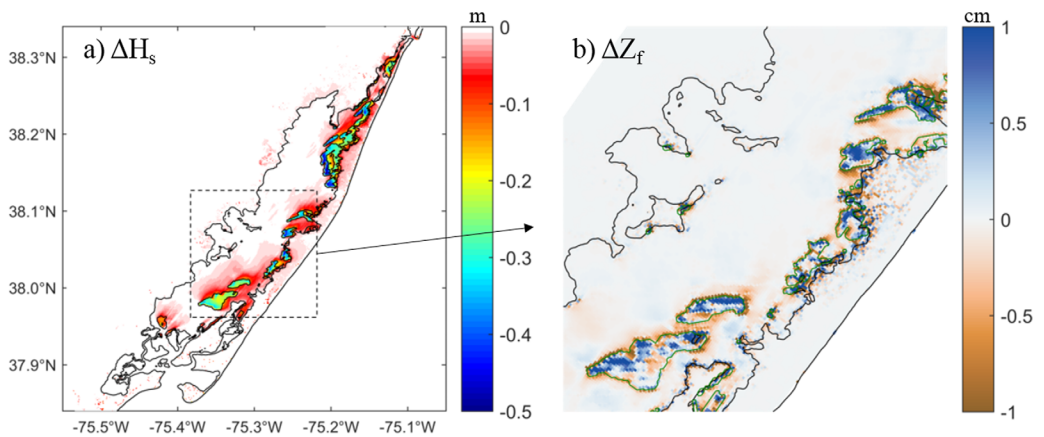

Figure 12. Influence of seagrass meadows (difference between the S and SAV scenarios) on (a) significant wave height at the instant of maximum wind stress and (b) sediment bed thickness at the end of Sandy (zoom). The seagrass meadows are outlined in green.

be approached with caution as the motions of flexible vegetation under wave oscillatory flows are not currently accounted for in SWAN. Further model developments are underway on the interactions between waves, currents, and flexible vegetation [*Beudin et al*., 2017].

While the present model might have overestimated wave height reduction, bed shear-stress and suspended sediment concentration were reduced by a factor 10 in the meadows, and by 10% on average in the bay. Total sediment fluxes (integrated during the 5 days of Sandy) were reduced by 15% on average in the bay with suspended and bedload fluxes in the meadows being reduced by a factor of 10 and 50, respectively, while they were enhanced around the meadows (up to an order of magnitude in the southern basin). In terms of bathymetric change, the presence of seagrass did not change the overall erosion/deposition patterns along the bay, but locally enhanced deposition on the meadows (without the presence of seagrass the shoals were erosional, Figure 9a) and induced erosion at the meadow edges (Figure 12b). Overall in the bay, the loss of sediment was reduced by 15% due to the presence of seagrass, but the bathymetric changes were increased by 50% (more important in the northern channel).

In summary, seagrass meadows had local effects on the hydrodynamics and sediment transport, in accordance with *Kombiadou et al*. [2014], yet their presence is extensive and perennial on the eastern flank of the bay, so they have the potential to stabilize the back-barrier shoals in regards to the long-term cumulative morphodynamic impact of storms. Seagrass meadows also have an ecological function in the bay as their presence decreases water flushing and suspended sediment concentration (turbidity), potentially modifying nutrient dynamics.

4.3. Model Limitations

The model results were compared with the three observed water level fluctuations time series available in Chincoteague Bay during Hurricane Sandy (Figure 2). Model skill during a later period (2014–2015) showed acceptable performance under less energetic conditions. No specific model tuning was conducted for the Hurricane Sandy simulations as the main objective was to understand the physical response to storm forcing.

Nevertheless, tidal fluctuations at Ocean City (Figure 2a) were overestimated by the model because the northern region of the Maryland Coastal Bays system (including Assawoman Bay, Saint Martin's River, and the Isle of Wight Bay) was not included in the present model domain [*Wang et al*., 2013; *Kang et al*., 2017]. However, as tidal amplitudes at Ocean City rapidly decrease in magnitude throughout the narrow Sinepuxent channel toward the interior of Chincoteague Bay, the misfit will also decrease.

Simulated subtidal fluctuations lagged behind the observations due in part to the large-scale model forcing in this area during Hurricane Sandy [*Warner et al*., 2017]. The main source of uncertainty in simulating storm conditions such as Hurricane Sandy is the available wind forcing. While the best available product was used for the present simulations, more local downscaling of wind conditions is often needed to achieve optimal model performance. No amount of model parameter adjustment can compensate for those deficiencies, as a better comparison with observations might be achieved but for the wrong reasons resulting in unrealistic physical response.

Other potential sources of model deficiency are related to inherent bottom roughness uncertainties (here based on uniform grain roughness, disregarding bed forms but including wave-induced roughness), the accuracy of the topo-bathymetry built on heterogeneous data sets, and the grid resolution in a domain characterized by particularly narrow channels and islands. A comprehensive quantification of the key sources of uncertainty in the hydrodynamic model remains to be completed. Many more sources of uncertainty are inherent in the sediment transport model and the associated errors often cascade resulting in a reduction in model skill for bed elevation changes [*Ganju et al*., 2017].

In general, the described model limitations tend to affect the solution locally, but the general character of the results is not expected to be globally altered. Despite the uncertainties, the model provided useful information about the importance of local heterogeneity in response to local/remote storm forcing for shallow-bay/barrier-island system behavior. In addition, the interpretation of the functional relationships between the model variables provided insight into the ability of the model to capture fundamental processes. In this regard, the model is considered acceptable for its intended use.

5. Conclusions

We applied a coupled ocean circulation, wave, and sediment transport numerical model (COAWST) to simulate the physical response of Chincoteague Bay to Hurricane Sandy. The dominant hydrodynamic processes inside the back-barrier bay were identified using a momentum balance approach and a set of complementary scenarios to investigate the contribution of each process. The model momentum balance during the storm was primarily between surface wind stress (local momentum source), horizontal pressure gradient force (acting as a remote forcing and often opposing the local wind stress), bottom friction (enhanced in shallower areas), and wave breaking (opposing the pressure gradient force especially along the eastern bay).

The model was verified against water level measurements at different locations in the bay, showing strong tidal attenuation but an (almost) unaltered subtidal signal. The response to subtidal coastal sea level fluctuations was mostly uniform throughout the bay, but wind-induced set-up/-down in the bay generated spatial and temporal variability that would not have been captured by a simplistic "bathtub" inundation model. The model was able to resolve the spatial heterogeneity in water level and provided estimates of the relative importance of the different processes (local versus remote wind and waves). While not a main factor affecting water level, local wind increased vertical mixing and horizontal exchange of water within the bay.

The contribution of the wave-induced setup at the inlets to sea level in the bay was 30% of the total peak value. While several studies have highlighted the importance of remote forcing to estuarine and bay water level response, in most cases they were unable to separate the effects of coastal sea level and wave set-up. The current model approach demonstrates the need for a proper wave characterization to evaluate the magnitude and timing of water level fluctuations in coastal bays.

The residence time during the storm was reduced up to 10 days (10–15% decrease from the average 2 months flushing time) in the proximity of the inlets. The along-bay exchange between sub-regions was limited (15–20% of floats were transported north-south), while larger cross-bay exchanges were estimated (50–60% of floats were transported in the east-west direction).

The bay served as a source of fine sediment to the inner continental shelf, while the ocean-facing barrier-island accumulated sand from landward overwash. Compared to the offshore region subjected to large waves, the back-barrier bay experienced relatively small bathymetric changes of the order of centimeters. Fine sediment from the bay was also deposited (less than 1 cm) over the extensive areas (increase in bay area up to 50%) inundated during the storm.

The presence of extensive seagrass resulted in minimal overall water level differences. Locally, seagrass dampened wave height by 30–75%, which decreased shoal erosion and reduced wave attack on the adjacent (within 1 km) marshes. Thus, seagrass contributed to an improved resilience of the back-barrier bay to storms.

While traditional approaches to the study of estuarine and coastal processes are based on observations and ocean circulation models, in this study we demonstrated that more complex approaches that consider not only currents, but also waves, sediments, and vegetation are needed to properly characterize the processes controlling back-barrier response to extreme events such as Hurricane Sandy.

Acknowledgments
This study was part of the Estuarine Physical Response to Storms project (GS2–2D), supported by the Department of Interior Hurricane Sandy Recovery program. We are grateful to Brian Andrews for his help with the topography and bathymetry data used to produce a continuous terrain model. We also thank Rich Signell and two anonymous reviewers for their feedbacks on the manuscript. Model metadata and output can be accessed at the USGS Coastal and Marine Geology Program data portal http://cmgdata.usgsportals.net/#.

References

Beudin, A., T. S. Kalra, N. K. Ganju, and J. C. Warner (2017), Development of a coupled wave-flow-vegetation interaction model, *Comput. Geosci.*, *100*, 76–86.

Blake, E. S., T. B. Kimberlain, R. J. Berg, J. P. Cangialosi, and J. L. Beven (2013), Tropical cyclone report Hurricane Sandy, *Tech. Rep. AL182012*, 157 pp., Tropical cyclone report, Hurricane Sandy, National Hurricane Center, Miami, Fla.

Booij, N., R. C. Ris, and L. H. Holthuijsen (1999), A third-generation wave model for coastal regions, part I: Model description and validation, *J. Geophys. Res.*, *104*(C4), 7649–7666.

Chant, R. J. (2001), Tidal and subtidal motion in a shallow bar-built multiple inlet/bay system, *J. Coastal Res.*, 32, 102–114.

Csanady, G. T. (1973), Wind-induced barotropic motions in long lakes, *J. Phys. Oceanogr.*, *3*, 429–438.

Defne, Z., and N. K. Ganju (2014), Quantifying the residence time and flushing characteristics of a shallow, back-barrier estuary: Application of hydrodynamic and particle tracking models, *Estuaries Coasts*, *38*(5), 1–16.

Defne, Z., N. K. Ganju, and A. Aretxabaleta (2016), Estimating time-dependent connectivity in marine systems, *Geophys. Res. Lett.*, *43*, 1193–1201, doi:10.1002/2015GL066888.

Eldeberky, Y., and J. A. Battjes (1996), Spectral modelling of wave breaking: Application to Boussinesq equations, *J. Geophys. Res.*, *101*(C1), 1253–1264.

Fagherazzi, S., and P. L. Wiberg (2009), Importance of wind conditions, fetch, and water levels on wave-generated shear stresses in shallow intertidal basins, *J. Geophys. Res.*, *114*, F03022, doi:10.1029/2008JF001139.
Ganju, N. K., and C. R. Sherwood (2010), Effect of roughness formulation on the performance of a coupled wave, hydrodynamic, and sediment transport model, *Ocean Modell.*, *33*, 299–313.
Ganju, N. K., S. E. Suttles, A. Beudin, D. J. Nowacki, J. L. Miselis, and B. D. Andrews (2017), Quantification of storm-induced bathymetric change in a back-barrier estuary, *Estuaries Coasts*, *40*(1), 22–36.
Garvine, R. W. (1985), A simple model of estuarine subtidal fluctuations forced by local and remote wind stress, *J. Geophys. Res.*, *90*(C6), 945–948.
Haidvogel, D. B., et al. (2008), Ocean forecasting in terrain-following coordinates: Formulation and assessment of the regional ocean modeling system, *J. Comput. Phys.*, *227*(7), 3595–3624.
Hapke, B. C. J., O. Brenner, R. Hehre, B. J. Reynolds, and S. Jewell (2013), Coastal change from Hurricane Sandy and the 2012–13 winter storm season: Fire Island, NY, *U. S Geol. Surv. Open File Rep., 2013–1231*, 37 p.
Irish, J. L., and R. Cañizares (2009), Storm-wave flow through tidal inlets and its influence on bay flooding, *J. Waterw. Port Coastal Ocean Eng.*, *135*(2), 52–60.
Kang, X., M. Xia, J. S. Pitula, and P. Chigbu (2017), Dynamics of water and salt exchange at Maryland Coastal Bays, *Estuarine Coastal Shelf Sci.*, *189*, 1–16.
Kombiadou, K., F. Ganthy, R. Verney, M. Plus, and A. Sottolichio (2014), Modelling the effects of *Zostera noltei* meadows on sediment dynamics: Application to the Arcachon lagoon, *Ocean Dyn.*, *64*, 1499–1516.
Kumar, N., G. Voulgaris, J. C. Warner, and M. Olabarrieta (2012), Implementation of the vortex force formalism in the coupled ocean-atmosphere-wave-sediment transport (COAWST) modeling system for inner shelf and surf zone applications, *Ocean Modell.*, *47*, 65–95.
Longuet-Higgins, M. S., and R. W. Stewart (1964), Radiation stresses in water waves; a physical discussion, with applications, *Deep Sea Res. Oceanogr. Abstr.*, *11*, 529–562.
Luhar, M., and H. M. Nepf (2011), Flow-induced reconfiguration of buoyant and flexible aquatic vegetation, *Limnol. Oceanogr.*, *56*(6), 2003–2017.
Madsen, O. S. (1994), Spectral wave–current bottom boundary layer flows, in *Proceedings of the 24th International Conference on Coastal Engineering*, pp. 384–398, Res. Counc., Kobe, Japan.
Miles, T., G. Seroka, J. Kohut, O. Schofield, and S. Glenn (2015), Glider observations and modeling of sediment transport in Hurricane Sandy, *J. Geophys. Res. Oceans*, *120*, 1771–1791, doi:10.1002/2014JC010474.
Miselis, J. L., B. D. Andrews, R. S. Nicholson, Z. Defne, N. K. Ganju, and A. Navoy (2016), Evolution of mid-Atlantic coastal and back-barrier estuary environments in response to a hurricane: Implications for barrier-estuary connectivity, *Estuaries Coasts*, *39*, 916–934.
Mukai, A. Y., J. J. Westerink, R. A. Luettich, Jr., and D. Mark (2002), Eastcoast 2001: A tidal constituent database for the western North Atlantic, Gulf of Mexico and Caribbean Sea, *Tech. Rep. ERDC/CHL TR-02–24*, U.S. Army Eng. Res. and Dev. Cent., Coastal and Hydraul. Lab., US Army Engineer Research and Development Center, Coastal and Hydraulics Laboratory, Vicksburg, Miss.
NOAA (2012), NAM-12 North America, NOAA Operational Model Archive and Distribution System, NOAA/NWS, College Park, Md. [Available at http://nomads.ncep.noaa.gov/.]
NOAA (2013), Hurricane/Post-Tropical Cyclone Sandy, 66 pp., Hurricane Sandy Assessment Report, NOAA, Silver Spring, Md.
Noble, M. A., W. W. Schroeder, W. J. Wiseman, H. F. Ryan, and G. Gelfenbaum (1996), Subtidal circulation patterns in a shallow, highly stratified estuary: Mobile Bay, Alabama, *J. Geophys. Res.*, *101*(C11), 689–703.
Olabarrieta, M., J. C. Warner, and N. Kumar (2011), Wave-current interaction in Willapa Bay, *J. Geophys. Res.*, *116*, C12014, doi:10.1029/2011JC007387.
Orth, R. J., D. J. Wilcox, J. R. Whiting, L. Nagey, A. K. Kenne, and E. R. Smith (2013), 2012 distribution of submerged aquatic vegetation in Chesapeake and Coastal Bays, Special scientific report #155, Virginia Institute of Marine Science, (VIMS), Gloucester Point, Va. [Available at http://web.vims.edu/bio/sav/sav12/index.html.]
Pawlowicz, R., B. Beardsley, and S. Lentz (2002), Classical tidal harmonic analysis including error estimates in MATLAB using T_TIDE, *Comput. Geosci.*, *28*, 929–937.
Phleger, F. B. (1969), Some general features of coastal lagoons, in *International Symposium on Coastal Lagoons (Origin, Dynamics, and Productivity)*, edited by A. Ayala-Castañares and F. B. Phleger, p. 1–26, UNAM-UNESCO, Mexico.
Pritchard, D. W. (1960), Salt balance and exchange rate for Chincoteague Bay, *Chesapeake Sci.*, *1*, 48–57.
Sherwood, C. R., J. W. Long, P. J. Dickhudt, P. S. Dalyander, D. M. Thompson, and N. G. Plant (2014), Inundation of a barrier island (Chandeleur Islands, Louisiana, USA) during a hurricane: Observed water-level gradients and modeled seaward sand transport, *J. Geophys. Res. Earth Surf.*, *119*, 1498–1515, doi:10.1002/2013JF003069.
Signell, R. P., R. C. Beardsley, H. C. Graber, and A. Capotondi (1990), Effect of wave-current interaction on wind-driven circulation in narrow, shallow embayments, *J. Geophys. Res.*, *95*(C6), 9671–9678.
Smith, N. P. (2001), Seasonal-scale transport patterns in a multi-inlet coastal lagoon, *Estuarine Coastal Shelf Sci.*, *52*, 15–28.
Suttles, S. E., N. K. Ganju, S. M. Brosnahan, E. T. Montgomery, P. J. Dickhudt, J. Borden, and M. A. Martini (2016), Oceanographic and water-quality measurements in Chincoteague Bay, Maryland/Virginia, 2014–2015, *U.S. Geol. Surv. Open File Rep.*, *2017–1032*, 95 pp., data release, [doi:10.5066/F7DF6PBV.]
SWAN Team (2015), SWAN (cycle III version 41.10A), SWAN Scientific and Technical Documentation, technical report, Delft Univ. of Technol., Delft, Netherlands. [Available at http://www.swan.tudelft.nl.]
Trembanis, A., C. DuVal, J. Beaudoin, V. Schmidt, D. Miller, and L. Mayer (2013), A detailed seabed signature from Hurricane Sandy revealed in bedforms and scour, *Geochem. Geophys. Geosyst.*, *14*, 4334–4340, doi:10.1002/ggge.20260.
USACE (2013), 2012 Post-Superstorm Sandy Lidar Elevation Data, USACE National Coastal Mapping Program, technical report. [Available at https://catalog.data.gov/dataset/2012-post-superstorm-sandy-lidar-elevation-data-usace-national-coastal-mapping-program.]
USGS (2015), The National Map, 3DEP products and services: The National Map, 3D Elevation Program Web page, technical report. [Available at http://nationalmap.gov/3dep_prodserv.html.]
Wang, H., Z. Wang, D. Loftis, and Y. Teng (2013), Hydrodynamic and water quality modeling and TMDL development for Maryland's Coastal Bays System, technical report, 224 pp., VIMS, Maryland Department of the Environment, Baltimore, Md.
Warner, J. C., C. R. Sherwood, H. G. Arango, and R. P. Signell (2005), Performance of four turbulence closure models implemented using a generic length scale method, *Ocean Modell.*, *8*, 81–113.
Warner, J. C., C. R. Sherwood, R. P. Signell, C. K. Harris, and H. G. Arango (2008), Development of a three-dimensional, regional, coupled wave, current, and sediment-transport model, *Comput. Geosci.*, *34*(10), 1284–1306.

Warner, J. C., B. Armstrong, R. He, and J. B. Zambon (2010), Development of a Coupled Ocean-Atmosphere-Wave-Sediment Transport (COAWST) modeling system, *Ocean Modell.*, *35*, 230–244.
Warner, J. C., W. C. Schwab, J. H. List, I. Safak, M. Liste, and W. Baldwin (2017), Inner-shelf ocean dynamics and seafloor morphologic changes during Hurricane Sandy, *Cont. Shelf Res.*, *138*, 1–18.
Wells, D. V., S. M. Harris, J. M. Hill, M. J. Park, and C. P. Williams (1997), The shallow sediments of upper Chincoteague Bay area in Maryland: Physical and chemical characteristics, *Md. Geol. Surv. Coastal Estuarine Geol. File Rep., 97–2*.
Wells, D. V., J. M. Hill, M. J. Park, and C. P. Williams (1998), The shallow sediments of the middle Chincoteague Bay area in Maryland: Physical and chemical characteristics, *Md. Geol. Surv. Coastal Estuarine Geol. File Rep., 98–1*, 104 pp.
Wells, D.V., R. A. Ortt, S. Van Ryswick, R. D. Conkwright, and K. A. Offerman (2004), Bathymetric survey of the Maryland portion of Chincoteague Bay, *Md. Geol. Surv. Coastal Estuarine Geol. File Rep. 04–04*, 29 pp.
Wong, K.-C. (1986), Sea-level fluctuations in a coastal lagoon, *Estuarine Coastal Shelf Sci.*, *22*, 739–752.
Wong, K.-C. (1987), Tidal and subtidal variability in Delaware's inland bays, *J. Phys. Oceanogr.*, *17*, 413–422.
Wong, K.-C., and J. E. Moses-Hall (1998), On the relative importance of the remote and local wind effects to the subtidal variability in a coastal plain estuary, *J. Geophys. Res.*, *103*(C9), 18,393–18,404.